Plastic and Moldable Metals by Self-Assembly of Sticky Nanoparticle Aggregates

Rafal Klajn, *et al.*

Science **316**, 261 (2007);
DOI: 10.1126/science.1139131

Science (print ISSN 0036-8075; online ISSN 1095-9203) is published weekly, except the last week in December, by the American Association for the Advancement of Science, 1200 New York Avenue NW, Washington, DC 20005.

pendent system of enzymatic reactions in a well-defined structural framework with a range of features that are not considered in single-enzyme catalysis. Moreover, detailed mechanistic questions regarding fatty acid synthesis by fungal FAS and related type I FAS enzymes (supporting online text) can now be addressed with structure-based genetic and biochemical experiments.

References and Notes

1. S. W. White, J. Zheng, Y. M. Zhang, C. O. Rock, *Annu. Rev. Biochem.* **74**, 791 (2005).
2. J. W. Campbell, J. E. Cronan, *Annu. Rev. Microbiol.* **55**, 305 (2001).
3. S. J. Wakil, J. K. Stoops, V. C. Joshi, *Annu. Rev. Biochem.* **52**, 537 (1983).
4. E. Schweizer, J. Hofmann, *Microbiol. Mol. Biol. Rev.* **68**, 501 (2004).
5. S. Smith, A. Witkowski, A. K. Joshi, *Prog. Lipid Res.* **42**, 289 (2003).
6. F. Lynen, *Eur. J. Biochem.* **112**, 431 (1980).
7. F. J. Asturias *et al.*, *Nat. Struct. Mol. Biol.* **12**, 225 (2005).
8. T. Maier, S. Jenni, N. Ban, *Science* **311**, 1258 (2006).
9. F. Wieland, E. A. Siess, L. Renner, C. Verfürth, F. Lynen, *Proc. Natl. Acad. Sci. U.S.A.* **75**, 5792 (1978).
10. J. K. Stoops, S. J. Kolodziej, J. P. Schroeter, J. P. Bretaudiere, S. J. Wakil, *Proc. Natl. Acad. Sci. U.S.A.* **89**, 6585 (1992).
11. S. J. Kolodziej, P. A. Penczek, J. K. Stoops, *J. Struct. Biol.* **120**, 158 (1997).
12. S. Jenni, M. Leibundgut, T. Maier, N. Ban, *Science* **311**, 1263 (2006).
13. Materials and methods are described in the supporting material on *Science* Online.
14. M. Leibundgut, S. Jenni, C. Frick, N. Ban, *Science* **316**, XXX (2006).
15. M. Ishikawa, D. Tsuchiya, T. Oyama, Y. Tsunaka, K. Morikawa, *EMBO J.* **23**, 2745 (2004).
16. R. N. Perham, *Annu. Rev. Biochem.* **69**, 961 (2000).
17. J. K. Stoops *et al.*, *J. Biol. Chem.* **253**, 4464 (1978).
18. F. Lynen, *Biochem. J.* **102**, 381 (1967).
19. A. M. Haapalainen, G. Merilainen, R. K. Wierenga, *Trends Biochem. Sci.* **31**, 64 (2006).
20. Y. Tang, C. Y. Kim, I. I. Mathews, D. E. Cane, C. Khosla, *Proc. Natl. Acad. Sci. U.S.A.* **103**, 11124 (2006).
21. L. Serre, E. C. Verbree, Z. Dauter, A. R. Stuitje, Z. S. Derewenda, *J. Biol. Chem.* **270**, 12961 (1995).
22. H. Engeser, K. Hübner, J. Straub, F. Lynen, *Eur. J. Biochem.* **101**, 407 (1979).
23. H. Engeser, K. Hübner, J. Straub, F. Lynen, *Eur. J. Biochem.* **101**, 413 (1979).
24. H. Schuster, B. Rautenstrauss, M. Mittag, D. Stratmann, E. Schweizer, *Eur. J. Biochem.* **228**, 417 (1995).
25. A. T. Keatinge-Clay *et al.*, *Structure* **11**, 147 (2003).
26. C. Oefner, H. Schulz, A. D'Arcy, G. E. Dale, *Acta Crystallogr. D Biol. Crystallogr.* **62**, 613 (2006).
27. V. S. Rangan, S. Smith, *J. Biol. Chem.* **272**, 11975 (1997).
28. A. C. Price, Y. M. Zhang, C. O. Rock, S. W. White, *Structure* **12**, 417 (2004).
29. A. C. Price, Y. M. Zhang, C. O. Rock, S. W. White, *Biochemistry* **40**, 12772 (2001).
30. Y. M. Qin *et al.*, *J. Biol. Chem.* **275**, 4965 (2000).
31. M. K. Koski, A. M. Haapalainen, J. K. Hiltunen, T. Glumoff, *J. Biol. Chem.* **279**, 24666 (2004).
32. K. M. Koski, A. M. Haapalainen, J. K. Hiltunen, T. Glumoff, *J. Mol. Biol.* **345**, 1157 (2005).
33. J. L. Fox, F. Lynen, *Eur. J. Biochem.* **109**, 417 (1980).
34. J. Y. Ha *et al.*, *J. Biol. Chem.* **281**, 18660 (2006).
35. P. A. Hubbard, X. Liang, H. Schulz, J. J. Kim, *J. Biol. Chem.* **278**, 37553 (2003).
36. R. J. Heath, C. O. Rock, *Nature* **406**, 145 (2000).
37. H. Marrakchi *et al.*, *Biochem. J.* **370**, 1055 (2003).
38. K. Werkmeister, R. B. Johnston, E. Schweizer, *Eur. J. Biochem.* **116**, 303 (1981).
39. S. E. Radford, E. D. Laue, R. N. Perham, S. R. Martin, E. Appella, *J. Biol. Chem.* **264**, 767 (1989).
40. R. N. Perham, *Biochemistry* **30**, 8501 (1991).
41. J. K. Stoops, S. J. Wakil, *Proc. Natl. Acad. Sci. U.S.A.* **77**, 4544 (1980).

42. All data were collected at the Swiss Light Source (SLS, Paul Scherrer Institute, Villigen). We are grateful to C. Schulze-Briese, S. Gutmann, E. Pohl, S. Russo, and T. Tomizaki for their outstanding support at the SLS. We thank T. Maier and J. Erzberger for critically reading the manuscript and all members of the Ban laboratory for suggestions and discussions; R. Grosse-Kunstleve, P. Afonine, and P. Adams for providing a prerelease version of the PHENIX refinement program and advice regarding structure refinement; A. Jones for a prerelease version of the program O; and D. Sargent for technical assistance. We thank A. Tsang for assembling *T. lanuginsosus* FAS contigs from expressed sequence tag sequence data produced by the Fungal Genomics Project (https://fungalgenomics.concordia.ca). This work was supported by the Swiss National Science Foundation (SNSF) and the National Center of Excellence in Research (NCCR) Structural Biology program of the SNSF. D.B. was supported by a Federation of European Biochemical Societies long-term fellowship. We thank the Electron Microscopy Center Zurich (EMEZ) for support. Coordinates and structure factors of the *T. lanuginosus* crystal structures have been deposited in the Protein Data Bank with accession codes 2UV9, 2UVA, 2UVB, and 2UVC. The cryoelectron microscopy map has been deposited at the EM Data Bank with accession code EMD-1338.

Supporting Online Material

www.sciencemag.org/cgi/content/full/316/5822/254/DC1
Materials and Methods
SOM Text
Figs. S1 to S19
Tables S1 to S7
References

1 December 2006; accepted 8 March 2007
10.1126/science.1138248

REPORTS

Plastic and Moldable Metals by Self-Assembly of Sticky Nanoparticle Aggregates

Rafal Klajn,[1]* Kyle J. M. Bishop,[1]* Marcin Fialkowski,[1] Maciej Paszewski,[1] Christopher J. Campbell,[1] Timothy P. Gray,[2] Bartosz A. Grzybowski[1,2]†

Deformable, spherical aggregates of metal nanoparticles connected by long-chain dithiol ligands self-assemble into nanostructured materials of macroscopic dimensions. These materials are plastic and moldable against arbitrarily shaped masters and can be thermally hardened into polycrystalline metal structures of controllable porosity. In addition, in both plastic and hardened states, the assemblies are electrically conductive and exhibit Ohmic characteristics down to ~20 volts per meter. The self-assembly method leading to such materials is applicable both to pure metals and to bimetallic structures of various elemental compositions.

Although various techniques have been developed to assemble nanoparticles at the microscale, such as nanoparticle superlattices (*1*, *2*) and three-dimensional crystals (*3*, *4*), scaling up these procedures to freestanding, macroscopic materials (*5*) has proven challenging. This situation contrasts with the formation of ceramic "greenwares" from colloidal particles such as clays, the interactions of which can hold the particles close together even during the dehydration and calcining steps that produce the final product (*6*). Here, we describe straightforward synthesis of such materials by a two-step method in which individual metal nanoparticles first self-assemble into deformable spherical aggregates ("supraspheres") and then "glue" together like pieces of clay into millimeter-sized structures. Notably, not only are these macroscopic materials plastic and moldable into arbitrary shapes, but they also can be electrically conductive. In addition, because of the metastability of the spherical building blocks, they can be thermally hardened and structurally evolved into porous, polycrystalline metal monoliths. The described methodology works well with nanoparticles of more than one type and can be used to prepare both pure-metal and bimetallic materials.

We used spherical nanoparticle assemblies, or supraspheres, similar to those prepared previous-

[1]Department of Chemical and Biological Engineering, Northwestern University, Evanston, IL 60208, USA. [2]Department of Chemistry, Northwestern University, Evanston, IL 60208, USA.

*These authors contributed equally to this work.
†To whom correspondence should be addressed. E-mail: grzybor@northwestern.edu

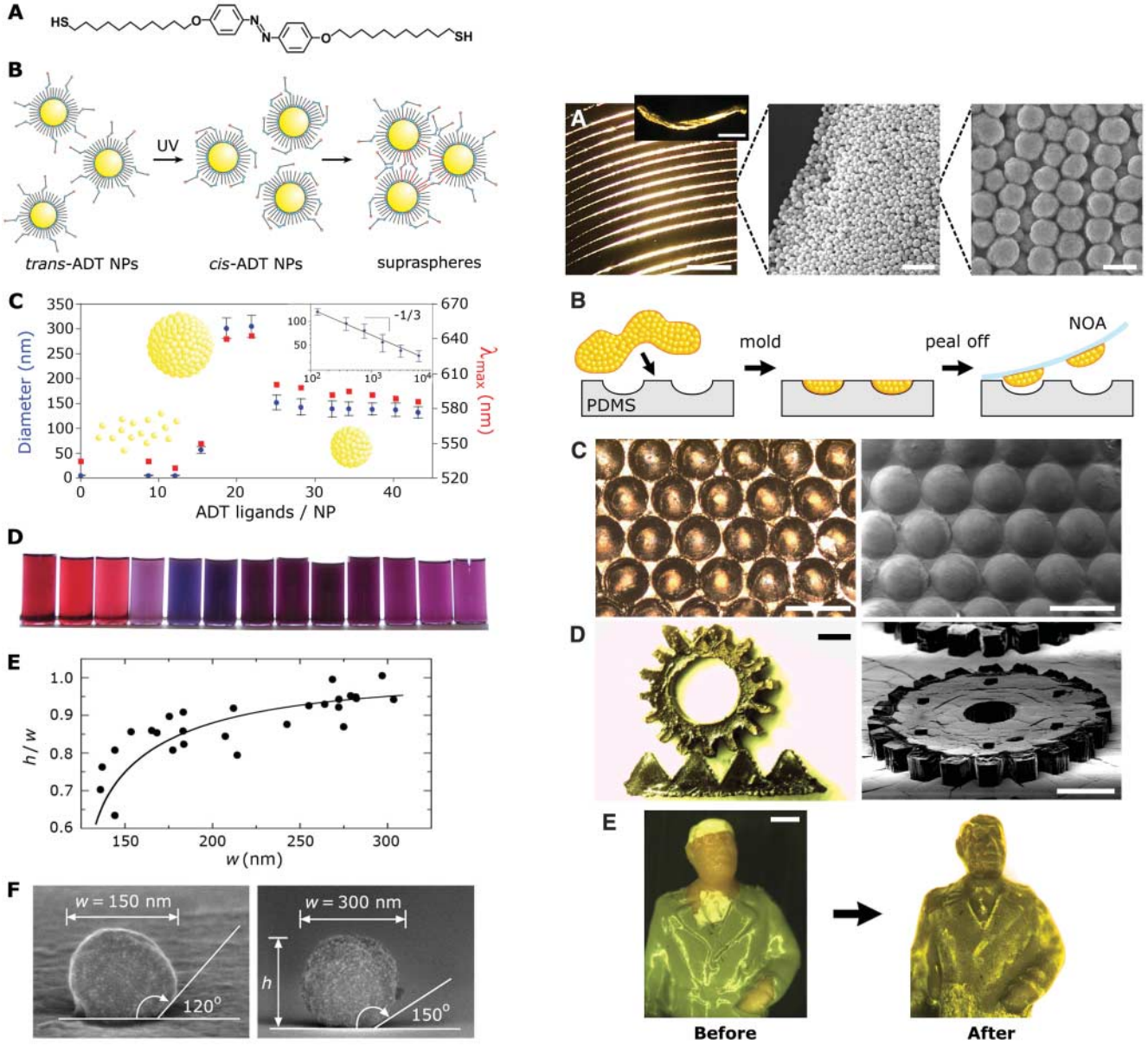

Fig. 1. Synthesis and properties of spherical nanoparticle aggregates. (**A**) Structure of the dithiol azobenzene cross-linker [4,4′-bis(11-mercaptoundecanoxy)azobenzene (ADT)] mediating self-assembly. (**B**) Scheme of the light-induced self-assembly of metal nanoparticles (NPs) coated with DDA and ADT into supraspheres (for mechanistic details of this process, see SOM text, sections 2 and 3). (**C**) Diameters (blue) and the wavelengths of maximal absorption (λ_{max}, red) for supraspheres formed by UV irradiation of Au nanoparticles (yellow) covered with various numbers of ADT ligands. Below the critical number of ligands adsorbed onto each nanoparticle (here, ~20), the photoinduced interactions between nanoparticles are too weak to cause their aggregation. Above this limit, nucleation and growth of supraspheres occurs. (Inset) Suprasphere diameters, D, decrease with increasing concentration of ADT ligands. The abscissa has the total ADT concentration (both adsorbed and free ligands) and is logarithmic to emphasize the agreement of the experimental results with $D \sim C_{ADT}^{-1/3}$ power law predicted by the nucleation-and-growth model (black line). Error bars show mean ± SD. (**D**) For metals exhibiting surface plasmon resonance (Au and Ag), aggregation is accompanied by a pronounced color change (as shown here for Au). The vials in the bottom row are solutions of supraspheres arranged in the order of increasing ADT/NP ratio and correspond to the points in the plot. (**E**) Aspect ratios of height to width, h/w, of supraspheres placed on silicon (100) increase with width. Solid line corresponds to the trend predicted by the Ramberg-Osgood model of suprasphere plasticity (for more details, see SOM text, section 4). (**F**) Side-view SEM images of two typical supraspheres on a silicon surface. **Fig. 2.** (**A**) Upon dewetting of a suprasphere solution from an inclined silicon surface, the supraspheres—similar to coffee dregs (*24*)—organize into bands. (Left) An optical micrograph of such bands ("wires") while still attached to the surface. Scale bar, 1 mm. (Inset) A freestanding wire washed off the surface with methanol. Scale bar, 0.5 mm. (Middle) SEM image showing the wire's porous structure. Scale bar, 1 μm. (Right) A magnification of individual supraspheres. Scale bar, 200 nm. (**B**) Concentrated solution of the supraspheres can be molded against masters [here, made of polydimethylsiloxane (PDMS)] of arbitrary surface reliefs and then peeled off onto a polyurethane film [Norland Optical Adhesive (NOA) no. 68]. (**C** and **D**) Optical and SEM images of microstructures prepared by molding Au or Ag supraspheres against an array of concave microlenses and an array of microgears. The freestanding gear and track pieces in the left panel of (D) were arranged manually after liberating from the polyurethane film. Scale bars, 200 μm. (**E**) Polypropylene miniature before (left) and after (right) coating with supraspheres. Scale bar, 1 mm.

ly (*7*–*9*). For our purposes, however, we required that the supraspheres be structurally sturdy as well as deformable and adhesive with respect to one another. We expected that these properties could be achieved by using long-chain dithiol cross-linkers (Fig. 1A), the terminal thiol (SH) groups of which are known to bind strongly to noble metal nanoparticles. The long spacer connecting these groups should endow the resulting aggregates with flexibility. In addition, our linkers incorporated a photoswitchable azobenzene unit that allowed for precise control of the assembly process and of the dimensions of the forming spheres by ultraviolet (UV) light.

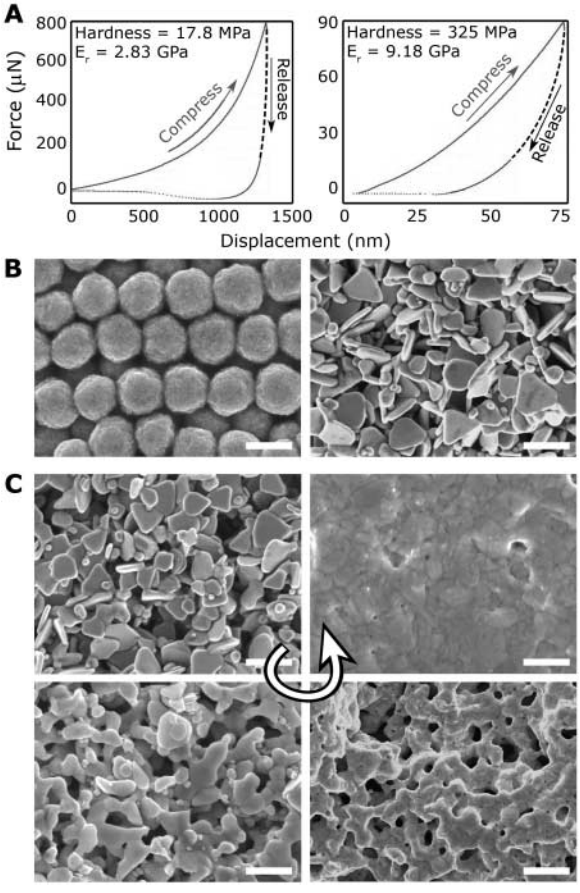

Fig. 3. (**A**) Typical load-displacement loops recorded during nanoindentation (TriboIndenter, Hysitron Inc.) of (left) a plastic wire (~1 mm by 170 μm by 30 μm) made of ~150-nm gold supraspheres and (right) the same wire after hardening at 50°C for 12 hours. The compression-release hysteresis recorded before hardening indicates plastic deformation. (**B**) SEM images corresponding to the graphs above show structural changes accompanying hardening. (**C**) Hardened materials subject to further heating at 350°C melt and shrink to ultimately give a solid block of metal. The panels show the progression, from top left, to bottom left, to bottom right, and finally to top right. Scale bars, 200 nm.

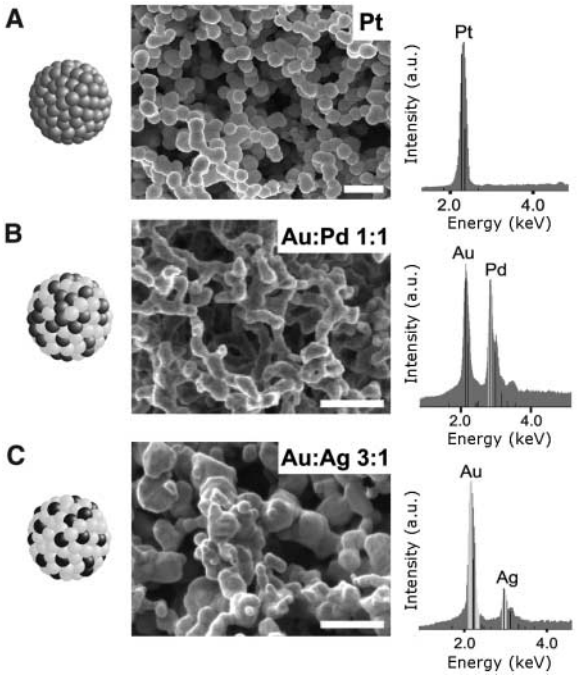

Fig. 4. Assembly schemes, SEM images, and energy dispersive analysis by x-rays (EDX) (Hitachi S3500) spectra of nanoporous materials made of (**A**) pure platinum, (**B**) 1:1 gold-palladium, and (**C**) 3:1 gold-silver. To verify spatially uniform composition of the bimetallic materials, EDX spectra were taken by focusing the beam at different regions of the same sample. a.u., arbitrary units. Scale bars, 500 nm.

In a typical procedure, we used 2 mM solutions of metal nanoparticles (here, mostly Au, but also Ag, Pt, or Pd) in toluene. The nanoparticles were ~5 nm in diameter and had a dispersity of $\sigma \approx 10\%$ [supporting online material (SOM) text, section 1]. We stabilized the solutions with 35 mM dodecylamine (DDA) capping agent and 10 mM didodecyldimethylammonium bromide (DDAB) surfactant. Next, under vigorous stirring, we added varying amounts (up to 2.4 mM) of photoactive trans-azobenzene dithiol (ADT) ligands (Fig. 1B) to the solutions. Because excess surfactant and capping agent prevented the spontaneous cross-linking of nearby nanoparticles through their divalent ADT ligands, the unirradiated solutions were stable (*10*) for many weeks. Low-power UV irradiation (365 nm, 0.7 mW/cm^2) (*11*) caused rapid trans-cis isomerization of the ADTs (Fig. 1B, center) and induced molecular dipoles on the azobenzene units [electric dipole moment (μ) = 4.4 debye for the cis (*12*) form compared with 0 debye for trans], causing the molecules to aggregate and cross-link into supraspheres (Fig. 1B, right). [For detailed discussion of the forces mediating self-assembly, see SOM text, sections 2 and 3.] The suprasphere growth occurred by means of a nucleation-and-growth mechanism, in which the free nanoparticles initially nucleated into small, thermodynamically stable clusters (unless smaller than a critical size) that subsequently grew by the addition of single nanoparticles until all nanoparticles available were used (*13*). The important feature of this mechanism is that it allowed the control of suprasphere diameters (Fig. 1C) by changing the concentration of the nanoparticles and/or the concentration of the ADT cross-linkers (*14*, *15*). In this way, we prepared supraspheres with diameters between about 50 and 300 nm (*16*) (Fig. 1, C and D, and fig. S6).

Irrespective of their sizes, the supraspheres were highly deformable upon contact with other spheres (or surfaces) and—despite being composed in ~92% weight by weight of metal (*17*)—had the mechanical properties of a plastic solid. The plasticity was confirmed in two ways: (i) by nanoindentation of individual supraspheres and (ii) by the aspect ratios and contact angles of spheres adhered onto different substrates, always increasing with increasing sphere size. Here, a systematic study of supraspheres on silicon (100) surfaces indicated (Fig. 1, E and F) that their deformation is driven by short-ranged adhesion forces, and can be described by the so-called Ramberg-Osgood model (*18*) of initial elastic response followed

by irreversible, plastic deformation (SOM text, section 4).

The plasticity and "stickiness" of the supraspheres enabled their further assembly into macroscopic materials (*19*). This is shown in Fig. 2, where suprasphere solutions either were dewetted from an inclined surface to leave behind an array of parallel "wires" (Fig. 2A) or were first concentrated to between 0.1 and 0.5% of the original volume and then molded against arbitrarily shaped and patterned masters (Fig. 2, B to E). Upon drying the solvent and washing with methanol to remove excess surfactant, the structures obtained could be gently pealed off the surface onto a polyurethane resin and then mechanically detached to give freestanding materials. Nanoindentation experiments revealed that similar to the supraspheres they comprise, these materials were plastic (with reduced modulus E_r of few gigapascals and hardness H of a few tens of megapascals; Fig. 3, A and B, left panels). At the same time, they could be structurally evolved and hardened by mild thermal treatment (about 50°C) to give relatively brittle, polycrystalline porous materials ($E_r \sim 10$ GPa and $H \sim 300$ MPa; Fig. 3, A and B, right panels). The plastic-to-porous metal evolution proceeded without noticeable changes in the materials' overall dimensions and was the result of gradual desorption of DDA and dithiol molecules (*20*, *21*) and consequent fusion of nearby nanoparticles composing the materials.

Because this process was similar for plastic precursors assembled from supraspheres of different sizes, it was possible to prepare hardened materials of different porosities. Scanning electron microscopy (SEM) analysis showed that the pore sizes were commensurate and increasing with increasing diameters, D, of the suprasphere building blocks. At the same time, surface areas of the porous materials decreased slightly with increasing D and, as evidenced by Brunauer-Emmett-Teller measurements, were typically several square meters per gram (e.g., 8 m^2/g for porous Ag made of 80-nm Ag supraspheres).

When hardening was continued at temperatures above 300°C, the pore sizes and the material's overall dimensions gradually decreased (by as much as 20%) to ultimately give a block of solid metal (Fig. 3C). During such heating, the material initially preserved its shape (up to about 10% shrinkage), but its fine structural details were lost upon full melting. Because of the adhesiveness of the supraspheres, they not only assembled with one another but also readily coated various glasses and plastics (e.g., rubber and polyurethanes such as Norland Optical Adhesive, SU-8 photoresist) dipped into suprasphere solutions. In one example of this capability (Fig. 2E), gold supraspheres formed uniform coating on a small polypropylene statuette.

In addition to plasticity, moldability, and susceptibility to thermal hardening, our evolving nanostructured materials exhibited electric properties reminiscent of semimetals. In both plastic and hardened states, these materials were electrically conductive; they had purely Ohmic current density-field strength characteristics over a range of applied electric fields from 2×10^5 V/m down to 20 V/m; and their resistance decreased as the underlying structure evolved (SOM text). The observed Ohmic characteristics are in sharp contrast to those of other metal-insulator structures studied to date, which usually require a threshold voltage (*22*, *23*) for conductance.

Because our self-assembly approach allows for the use of different types of suprapherical building blocks, all of the discussed methods and material properties could be extended to nanostructured materials composed of more than one metal—that is, to bimetallic materials (Fig. 4). In principle, such materials could be made either from mixtures of supraspheres of different types (e.g., all Au and all Pt) or from mixed supraspheres composed of different types of nanoparticles. In practice, however, the first method proved unsatisfactory because the different metals often phase separated upon thermal hardening. In contrast, hardening of mixed supraspheres gave structurally uniform materials (on the scale of ~100 nm), in which the composition at every probed location was equal to that of the supraspheres used. In this way, we were able to prepare bimetallic monoliths of various combinations and proportions of Au, Ag, Pt, and Pd. Two representative examples—Au and Pd (1:1) and Au and Ag (3:1)—are shown in Fig. 4, B and C. We believe that because of their high porosity, these materials may find uses in separations science and in heterogeneous catalysis, in which the application of multicomponent "nanofoams" to catalyze multiple (or multistep) reactions seems particularly interesting.

References and Notes

1. C. J. Kiely *et al.*, *Nature* **396**, 444 (1998).
2. E. V. Shevchenko *et al.*, *Nature* **439**, 55 (2006).
3. A. M. Kalsin *et al.*, *Science* **312**, 420 (2006).
4. C. B. Murray, C. R. Kagan, M. G. Bawendi, *Science* **270**, 1335 (1995).
5. F. Stellacci, *Nat. Mater.* **4**, 113 (2005).
6. W. D. Kingery, H. K. Bowen, D. R. Uhlmann, *Introduction to Ceramics* (Wiley, New York, 1976).
7. A. K. Boal *et al.*, *Nature* **404**, 746 (2000).
8. I. Hussain, Z. X. Wang, A. I. Cooper, M. Brust, *Langmuir* **22**, 2938 (2006).
9. M. M. Maye *et al.*, *J. Am. Chem. Soc.* **127**, 1519 (2005).
10. Excess DDA and DDAB helped to minimize van der Waals (vdW) forces between the nanoparticles by reducing the dielectric contrast ($\Delta\varepsilon$) between the nanoparticles and the solvent. Without this stabilizing effect, the magnitude of vdW interactions could be greater than k_BT, where k_B is the Boltzmann constant and T is temperature (e.g., with a Hamaker constant $A = 0.4 \times 10^{-21}$ J for interacting alkane-chain molecules in toluene, $E_{vdw} \sim 2k_BT$), and the nanoparticles would clump even in the absence of irradiation. Indeed, we verified experimentally that without excess DDA and DDAB, the nanoparticle solutions are unstable and precipitate rapidly to give disordered, black-powder aggregates.
11. Low-power irradiation for periods of up to several tens of minutes did not cause desorption of the thiols from nanoparticle surfaces. With more intense sources of UV light (>50 mW/cm^2) or at elevated temperatures, however, desorption was observed, and the nanoparticles coalesced into larger particles and aggregates that precipitated from solution.
12. X. Tong, G. Wang, A. Soldera, Y. Zhao, *J. Phys. Chem. B* **109**, 20281 (2005).
13. The nucleation-and-growth mechanism applies to this system only at short time scales, during which the supraspheres assemble by means of dipole-dipole interactions to consume all free nanoparticles in solution. At longer time scales, the suprasphere aggregates become "cemented" by dithiol cross-links and cannot coalesce with one another to achieve full phase separation.
14. Because the number of nucleation sites is proportional to the concentration of ADT, the suprasphere diameter scales with the concentration of ADT as $D \sim C_{ADT}^{-1/3}$.
15. D. Kashchiev, *Nucleation: Basic Theory with Applications* (Butterworth-Heinemann, New York, 2000).
16. Light-controlled self-assembly gave supraspheres of smaller size dispersity than alternative methods described in the literature (*7*–*9*). Also, we verified that spheres connected by shorter dithiol ligands were less "sticky" and required prolonged heating at high temperatures in order to self-assemble into larger structures. These properties made such supraspheres unsuitable for the molding experiments we conducted.
17. Metal weight percent was estimated from that of underlying gold nanoparticles. Specifically, for a spherical core-shell nanoparticle with a core of radius $R_c \sim 2.8$ nm and density $\rho_c = 19.3$ g/cm^3 (for gold) and with a self-assembled monolayer (SAM) of thickness ~1.4 nm and density $\rho_{SAM} \sim 0.73$ (for linear hydrocarbons), the weight percentage of metal may be estimated as $\rho_c R_c^3 / [\rho_c R_c^3 + \rho_{SAM}(R_{SAM}^3 - R_c^3)] \sim 0.92$. Similar values are expected for other noble metals.
18. H. W. Haslach Jr., R. W. Armstrong, *Deformable Bodies and Their Material Behavior* (Wiley, New York, 2004).
19. When nanoparticles were simply cross-linked without forming the intermediate supraspheres, they formed precipitates that could not be assembled, molded, or hardened.
20. D. V. Leff, P. C. Ohara, J. R. Heath, W. M. Gelbart, *J. Phys. Chem.* **99**, 7036 (1995).
21. H. M. Schessler, D. S. Karpovich, G. J. Blanchard, *J. Am. Chem. Soc.* **118**, 9645 (1996).
22. For metal/insulator structures of dimensions comparable to our supraspheres, the threshold voltages reported were on the order of ~2×10^6 V/m [e.g., (*23*)].
23. A. Beck *et al.*, *Appl. Phys. Lett.* **77**, 139 (2000).
24. R. D. Deegan *et al.*, *Phys. Rev. E Stat. Phys. Plasmas Fluids Relat. Interdiscip. Topics* **62**, 756 (2000).

25. We thank M. Ratner and G. C. Schatz for helpful discussions, as well as S. Smoukov for his help with nanoindentation experiments. This work was supported by the NSF CAREER (CTS-0547633) Award, 3M Non-Tenured Faculty Award, the Pew Scholarship, and the Sloan Fellowship (to B.A.G.). R.K. was supported by the NSF under the Northwestern Materials Research Science and Engineering Center Award. K.J.M.B. was supported by the NSF Graduate Fellowship. C.J.C. was supported by a Northwestern University Presidential Fellowship.

Supporting Online Material

www.sciencemag.org/cgi/content/full/316/5822/261/DC1
SOM Text
Figs. S1 to S6
References

21 December 2006; accepted 6 March 2007
10.1126/science.1139131